The toughening of polyamide-6 by brominated poly(isobutylene-*co*-*p*-methylstyrene): fracture and toughening mechanisms

Dongming Li and A. F. Yee*
Department of Materials Science and Engineering, University of Michigan, Ann Arbor, MI 48109, USA

and K. W. Powers, H.-C. Wang* and T. C. Yu
Exxon Chemical Company, PO Box 45, Polymers Group, Linden, NJ 07036, USA
(Received 21 January 1993)

A study on the toughening of polyamide-6 (PA-6) with a new elastomeric modifier, brominated poly(isobutylene-*co*-*p*-methylstyrene) (BrXP-50), was conducted. Morphological analyses and mechanical tests were combined to evaluate the toughening mechanisms of modified PA-6 and the fracture mechanism of unmodified PA-6. We conclude that the fracture mechanism of unmodified PA-6 in the impact test is crazing–cracking under the dilatational stress created by the plastic constraint, while that of the BrXP-50 elastomer modified PA-6 is plastic tearing limited by the ultimate tensile strain. Cavitation of BrXP-50 elastomer particles occurred in the impact test, and is proposed as a controlling step in toughening: it relieves the plastic constraint so that the cracking process is postponed and additional plastic deformation can occur, leading to higher impact toughness.

(Keywords: toughening; impact fracture; cavitation)

INTRODUCTION

Improving the toughness, especially the impact toughness, of polyamides by the incorporation of elastomeric particles has been widely practised over the past two decades[1,2], but the underlying toughening mechanisms are not yet fully understood. The subject is still challenging. The following parameters are considered to be influential factors: (i) impact modifier concentration; (ii) impact modifier size; (iii) interparticle distance; (iv) mechanical properties of the modifiers; (v) polyamide matrix structure and properties; and (vi) adhesion between impact modifiers and the polyamide matrix. A key question, however, has yet to be answered: What is the most important function of elastomeric modifiers in toughening?

Some possible functions of the modifiers in the toughening of polymers could be[3,4]: (i) stretching and tearing; (ii) to cause multiple crazing; (iii) to create stress concentration and induce the shear yielding of the matrix; and (iv) cavitation and the induction of shear yielding and plastic dilatation.

The first function, stretching and tearing, can be excluded because it has been shown that matrix deformation is the major dissipation mechanism in the toughening of polyamides[5]. As for the importance of multiple crazing in the toughening of polyamides, there is not yet full agreement among investigators[6–8].

Narisawa and Ishikawa[6] studied crazing in unmodified polyamide-6 (PA-6) in a low speed plane strain bending condition. They observed crazes at the tip of the local plastic zone ahead of the notch, and proposed a mechanism where crazing occurs under a dilatational stress which builds up as a result of 'plastic constraint'. The crazes will eventually change to a crack and lead to the failure of the specimen. These investigators believe that crazing is an important source of toughness in modified semicrystalline thermoplastics such as propylene–ethylene block copolymer. However, they did not investigate the importance of crazing in impact toughening. Wu[7], citing evidence from transmission electron microscopy (TEM) on modified PA-66, stated that extensive crazing occurs in the polyamide matrix within the energy dissipation zone, and multiple crazing contributes substantially to the impact strength of elastomer-modified polyamide. By comparing the difference in the enthalpy content between an undeformed specimen and a stress-whitened specimen from an impact fracture, and by assuming that this difference results entirely from the surface energy component of crazes, Wu estimated that about 25% of the total impact energy dissipation came from crazing. On the other hand, Ramsteiner and Heckmann[8] studied the fracture mode of rubber-modified PA-6 in the temperature range between its secondary transition and glass transition, and reported no crazing could be found either by TEM or optical microscopy. These researchers did, however, report the occurrence of cavitation of the rubber particles.

*To whom correspondence should be addressed

0032-3861/93/214471-10

Several researchers[9,10] have postulated that the effectiveness of a modifier originates from its ability to cause stress concentration. The stress concentration alone will lead to local nucleation of shear yielding. When modifier particles are sufficiently close together their stress fields will overlap, creating enhanced stress fields around modifier particles which cause additional shear yielding. More specifically, Hobbs *et al.*[9] proposed that by counting the number of interactions, the brittle–tough (BT) transition dependent only on modifier concentration and particle size can be predicted. Wu[10], however, proposed that the interparticle distance (ID) controls the BT transition, and the critical interparticle distance (ID_c) is a property of the matrix, independent of the particle size and volume fraction of modifiers. Neither Hobbs *et al.* nor Wu consider rubber cavitation to be important.

According to the explanations set forth by Hobbs *et al.* and by Wu, the toughening effect of different modifiers will be the same if their stress concentration effect is the same. Both groups implicitly assume that good adhesion between the toughness and the matrix exists. Oxborough and Bowden[11] had previously demonstrated that, as long as the shear moduli of different elastomeric modifiers are less than one tenth the shear modulus of the matrix polyamide, their stress concentration effects will be the same. Thus, their toughening efficiency should be the same. Other researchers[12–14], however, have shown that the toughening effect varies with the modifier type even when the volume concentrations and particle sizes of modifiers were kept the same, and the shear moduli of the modifiers were all less than one tenth the shear moduli of the matrices. This contradicts the notion that the stress concentration effect of the elastomeric particles is the only source of increased toughness. Further, in the stress concentration explanation, only the shear stress concentration is considered, while the hydrostatic stress (which is the cause of fracture in constrained polymer bodies) is totally neglected.

The cavitation of rubber particles has been shown to be a very important step in the toughening of some rubber-modified polymers, such as epoxy and polycarbonate[3,15,16]. Rubber cavitation is believed to relieve the local hydrostatic tension so that fracture due to crazing–cracking is postponed or prevented, and the matrix polymer deforms in a less constrained state. If the rubber concentration is sufficiently high, cavitation can give rise to a state of plane stress. Thus enhanced, massive shear yielding can take place, resulting in large amounts of energy absorption. Ramsteiner and Heckmann[8] reported that the fracture mode of rubber-modified PA-6 between the temperatures of its secondary transition and glass transition was mainly given by shear processes accompanied by voiding inside the rubber particle (rubber cavitation). Similar observations of rubber cavitation were made by Ban *et al.* in ethylene-*co*-propylene rubber-modified PA-66[17]. The cavitation concept has also been evaluated by using several different rubber-modified PA-6s, and it was found that a correlation exists between the cavitation initiation stress of the rubbers and the impact strength of the modified materials[18].

In this paper we report our studies on the toughening of PA-6 by a new elastomeric toughener, brominated poly(isobutylene-*co*-*p*-methylstyrene) (BrXP-50), produced by the Polymers Group of the Exxon Chemical Company. Morphological analyses and mechanical tests were combined to evaluate the toughening mechanism of modified PA-6 as compared with the fracture mechanism of unmodified PA-6.

EXPERIMENTAL

Materials

The matrix material used in this research was Capron 8209F, which is a PA-6 in pellet form produced by Allied Signal Inc. The elastomeric modifier was poly(isobutylene-*co*-*p*-methylstyrene) (BrXP-50), prepared by the Polymers Group of the Exxon Chemical Company.

The poly(isobutylene-*co*-*p*-methylstyrene) was prepared by carbocationic copolymerization of isobutylene (IB) and *p*-methylstyrene (PMS). It has a saturated copolymer backbone chain with randomly distributed, pendent *p*-methyl substituted aromatic rings. After polymerization, a solution bromination process was used in which some of the *p*-methyl groups were converted to bromomethyl groups to provide the desired benzyl bromide functionality. The structure of BrXP-50 is discussed in more detail in ref. 2. The BrXP-50 elastomer used in the present study had a viscosity average molecular weight of 460 000, determined in diisobutylene at 20°C, and a Mooney viscosity of 52 (M_L 1+8 at 125°C). It contained 2.3 mol% PMS of which 0.4 mol% was brominated. The actual bromine in the BrXP-50 elastomer was 0.7 wt%, determined by X-ray fluorescence.

The benzylic bromines of BrXP-50 elastomer possess excellent thermal stability and are able to react with the amine end-group or the amide groups of the polyamides. A strong bonding between the elastomer and the polyamide matrix is possible. The thermal stability and chemical reactivity make BrXP-50 an ideal candidate for alloying with high melting point polyamides.

Compounding processes and machining of test specimens

All experimental samples were compounded using a 2 cm Welding Engineers counter-rotating twin-screw extruder fitted with a strand die, a cooling water bath, and a pelletizer. A stream of nitrogen was introduced to provide an inert atmosphere and to purge reaction by-products. This was followed by a downstream vent zone to collect any further reaction by-products.

PA-6 pellets were dried in a dehumidifier oven at 60°C for four hours before compounding. BrXP-50 elastomer was first granulated into pellets approximately 5 mm in diameter. A small amount of PA-6 powder was introduced as an antisticking agent during granulation to prevent agglomeration. For compounding runs where a basic metal promoter was used, the metallic oxide was introduced as the antisticking agent. PA-6 and BrXP-50 granules were dry blended at various weight ratios and then metered into the feed throat of the extruder using a K-Tron screw feeder.

The finished pellets were dried for four hours at 60°C using the same dehumidifier/dryer before being converted into test specimens with a Boy 15/5 injection moulding machine.

Mechanical testing

The test specimens produced as above were stored in metal cans before they were tested to obtain data for the dry, as-moulded samples. Notched Izod impact tests were

conducted according to ASTM D256 in the temperature range −40 to 25°C. The instrument used was an ICI instrumented impact tester with a custom-made temperature chamber. The average values from at least five tests are reported. The geometry of a standard Izod impact test specimen was: length $L = 70$ mm, width $W = 12.54$ mm, thickness $B = 3.18$ mm, notch depth $a = 2.54$ mm, and radius of notch base $R = 0.25$ mm. The specimens were directly tested in the temperature chamber. Temperature equilibration was assumed by monitoring the temperature of a dummy specimen in the chamber with a thermocouple.

Uniaxial tensile tests were conducted with an Instron 4502 at a crosshead speed of 50 mm min^{-1} at room temperature. ASTM D638 type I dumb-bell-shaped specimens were used. The geometry of such a specimen was: gauge length $L_0 = 55$ mm, overall length $L = 165$ mm, gauge width $W_0 = 12.54$ mm, overall width $W = 19$ mm, and thickness $B = 3.175$ mm.

Microscopy analysis

To reveal the deformation mechanisms in the damage zone of an impact-tested specimen, a combination of optical microscopy (OM), scanning electron microscopy (SEM) and transmission electron microscopy (TEM) was used.

Optical microscopy was used to examine the subsurface damage of impact-fractured specimens, and to define the size of the shear plastic deformation zone. A thin section perpendicular to the fracture surface was obtained by petrographic thinning techniques, which involved embedding the damage zone portion of the specimen in a clear epoxy resin, then reducing the thickness by a combination of cutting and polishing until a final thickness of 25 μm or less was reached. The sections thus obtained were examined under a Nikon research microscope, with or without crossed polarizers.

For BrXP-50 elastomer-modified PA-6 specimens fractured at room temperature, the damage zone showed very intense light scattering. Even though a thin section of 25 μm or less was made according to the procedure mentioned earlier, the light scattering was so strong that no plastic birefringence could be observed except at the fracture surface. To identify the cause of this strong light scattering and to reveal the actual size of the plastic birefringence zone, we subjected some of the impact-tested specimens to hydrostatic pressure before making the thin sections, and this eliminated the strong light scattering. Furthermore, the birefringent plastic zone was now clearly revealed. The high pressure apparatus we used was a porosimeter from Micrometrics, and the pressure we used was 200 MPa. The success of this technique suggests that the light scattering is due to the existence of numerous submicron-sized to micron-sized voids. Further discussion of these results is given in a later section.

SEM was used to (i) determine the impact modifier size, and (ii) examine the fracture surfaces. To determine the impact modifier size and distribution, smooth surfaces of impact-modified PA-6 materials were prepared by cryogenic microtoming with a diamond knife using a Reichert–Jung ultramicrotome. Then, the elastomeric modifier was extracted from the surface by etching with boiling xylene overnight. After sputter coating with a thin film of gold, the specimens were examined in a Hitachi S-800 scanning electron microscope. Particle analysis was then performed on the SEM micrographs by using the Image 1.47® commercial image analysis package.

TEM was used to provide morphological information on the impact modifiers, especially the type of deformation they suffered after impact testing. Thin sections were prepared by cryogenic microtoming. These ultra-thin sections were then stained with RuO_4 to enhance the contrast between PA-6 matrix and BrXP-50 modifier. The instrument used was a JEOL 2000FX transmission electron microscope.

Differential scanning calorimetry (d.s.c.) analysis

D.s.c. was used to analyse the crystallization behaviour of pure and BrXP-50 elastomer modified PA-6 to determine whether the addition of BrXP-50 elastomer changed the crystalline structure of the PA-6 matrix. The crystal melting point and heat of fusion were measured at a 10°C min^{-1} heating rate using a Perkin–Elmer DSC-7. The crystallinity in the as-moulded condition was measured in the first run. After that, the samples were kept at 30°C above the melting point for three minutes, quenched down to room temperature, and were then subjected to the second run. These procedures provided the specimens with a uniform thermal history. Both sets of results were used to evaluate the effect of BrXP-50 elastomer on the crystallization behaviour of PA-6.

RESULTS AND DISCUSSION

Mechanical properties of pure and BrXP-50 elastomer modified PA-6

Table 1 gives the general mechanical properties of pure and BrXP-50 elastomer modified PA-6. Notched Izod impact strength profiles at different temperatures were obtained for samples containing various amounts of BrXP-50 elastomer. The impact resistance was plotted against test temperature, resulting in the familiar sigmoid-shaped curves (*Figure 1*). The toughening effect is indicated by the fact that the impact strengths of

Table 1 Mechanical properties of pure and BrXP-50 elastomer modified PA-6

Material composition		Tensile modulus (MPa)	Yield stress (MPa)	Elongation at yield (%)	Elongation at break (%)	Notched Izod impact strength (J m^{-1})				
PA-6	BrXP-50					23°C	0°C	−10°C	−20°C	−30°C
100	0	1234	42.7	4.1	467.5	59	27	23	27	29
95	5	1214	44.8	3.9	306.1	174	98	80	88	70
90	10	1138	40.7	3.9	263.5	716	141	114	109	83
80	20	931	31.7	3.8	96.4	1128	880	183	139	92
70	30	696	24.4	3.6	67.3	1167	1094	1134	887	160

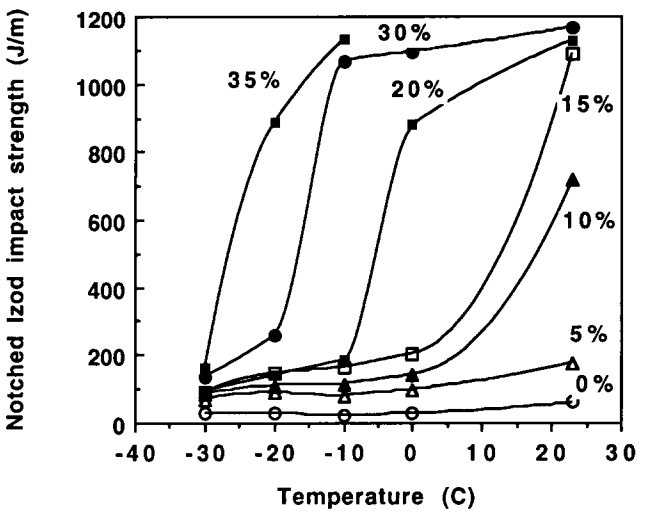

Figure 1 Impact strength of PA-6/BrXP-50 elastomer blends as a function of temperature

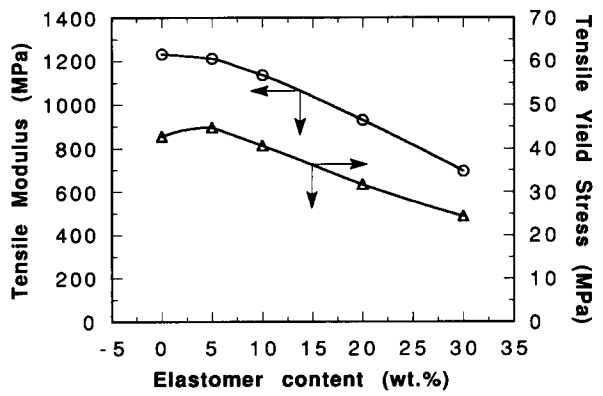

Figure 2 Tensile modulus and yield stress of PA-6/BrXP-50 elastomer blends *versus* elastomer content

BrXP-50 elastomer modified PA-6 are larger than those of the pure PA-6 both before and after brittle–tough (BT) transition. The same effect is revealed when the BT transition temperature shifts to lower temperatures as the rubber concentration increases.

Tensile properties of both pure and BrXP-50 elastomer modified PA-6 show that BrXP-50 elastomer reduces the tensile modulus, tensile yield stress, elongation at yield and elongation at break. The changes in tensile modulus and yield stress *versus* BrXP-50 elastomer content at room temperature are shown in *Figure 2*. Note that with the addition of 20 wt% BrXP-50 elastomer, the yield stress drops to about 75% of that of unmodified PA-6.

Particle analysis and thermal analysis results

By using the particle analysis method introduced earlier, the mean diameter of BrXP-50 elastomer particles in the blends was found to be 0.52 μm, with a standard deviation of 1.38 μm. The particle size and dispersion are little changed as the elastomer content increases, indicating that they were determined by the interaction between the two components and the processing condition.

D.s.c. was used to analyse the melting behaviour of BrXP-50 elastomer modified PA-6, and the results are shown in *Figures 3* and *4*. The temperature of the melting peak changes very little with the addition of BrXP-50 elastomer. The apparent heat of fusion decreases slightly with increasing elastomer content. Normalizing the heat of fusion with the PA-6 content results in very little change of the heat of fusion *versus* the elastomer content. Thus, the total amount of crystallinity is not affected by the elastomer content. These results, however, are inconclusive regarding the nature of the crystallinity and how it might be affected by the reaction between the two components.

Cavitation and shear yielding revealed by microscopy analysis

The coexistence of volume dilatation and plastic shear processes. Thin sections made in the manner described in the Experimental section were obtained perpendicular to the impact fracture surface and were examined with an optical research microscope with or without crossed polarizers. The resulting optical micrographs for a PA-6/BrXP-50 95/5 specimen fractured at 20°C (just below the BT transition temperature) are shown in *Figure 5*. The damage zone includes a localized light-scattering zone which is followed by brittle failure. The light-scattering zone has a thin layer of birefringence evident at the fracture surface. The size of the light-scattering zone increases with elastomer content and testing temperature. For 10 wt% or more BrXP-50 elastomer modified PA-6 specimens tested at room temperature, the damage zone covers the entire specimen ligament (*Figure 10*). It is very important to know the cause of the strong light scattering, and how big the shear plastic deformation (birefringence) zone is. The latter is impossible to ascertain due to the light scattering.

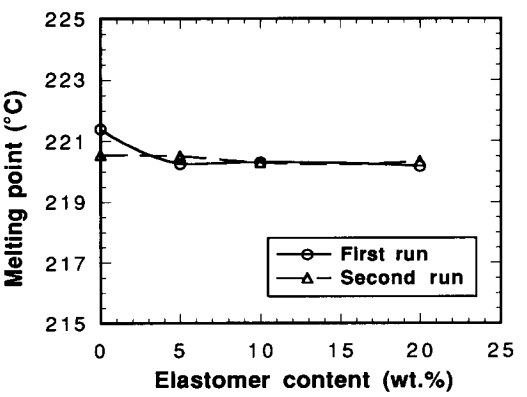

Figure 3 Peak melting temperature of PA-6/BrXP-50 blends *versus* elastomer content

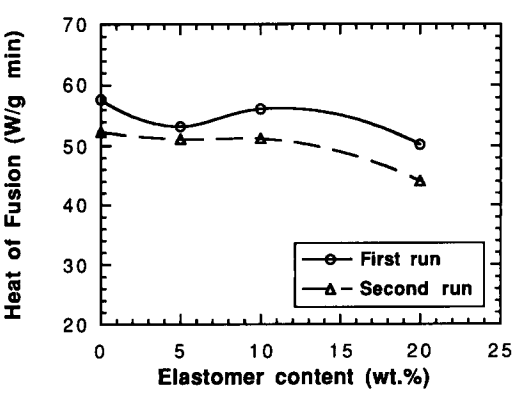

Figure 4 Heat of fusion of PA-6/BrXP-50 blends *versus* elastomer content

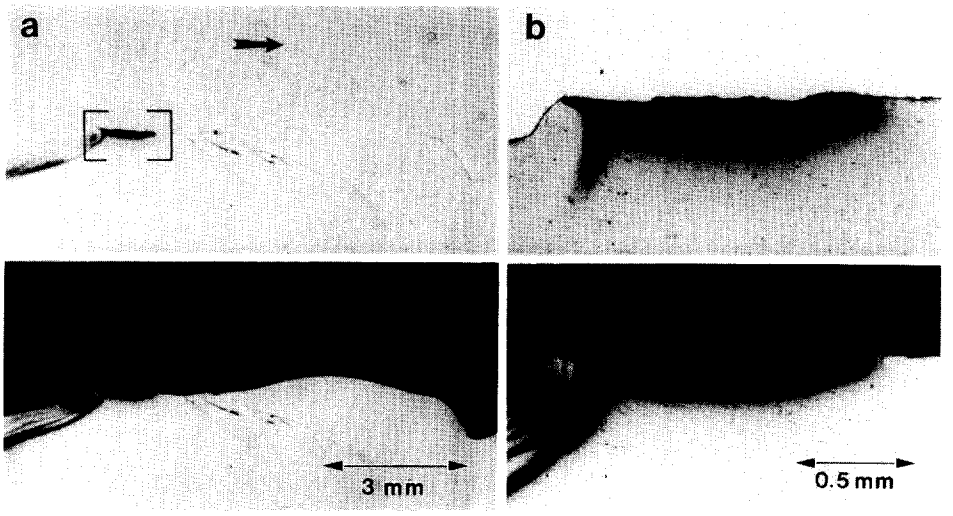

Figure 5 Optical micrographs of a thin section perpendicular to the fracture surface of a PA-6/BrXP-50 95/5 specimen fractured at 20°C: (a, b) without crossed polarizers; (c, d) with crossed polarizers

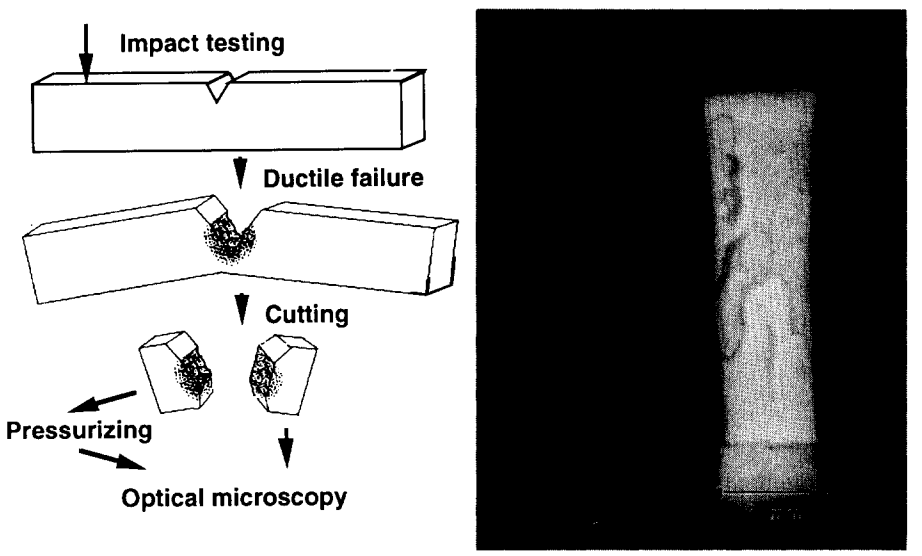

Figure 6 Illustration of thin sectioning and pressurizing procedure and an optical micrograph of pressurized and unpressurized specimens of a PA-6/BrXP-50 70/30 blend

Internal voids such as cavities or crazes are the usual causes of light scattering and they can be closed by applying a hydrostatic pressure. We pressurized an impact-fractured specimen containing 30 wt% BrXP-50 elastomer by using mercury, which has no solvent effect on the pressurized material, as the pressure-transmitting fluid. The hydrostatic pressure we used was 200 MPa, which is about five times the yield stress of this material and is certain to close any internal voids. Pressurization virtually eliminated the strong light scattering (*Figure 6*), indicating that it is indeed due to volume dilatation processes such as cavity or craze formation. The SEM and TEM studies described in the next section demonstrate that cavitation in the BrXP-50 elastomer particle is the source of light scattering.

Cavitation evidenced by SEM and TEM analysis. The existence of a localized volume dilatation process in the form of either cavitation or crazing was identified by optical microscopy. SEM and TEM analyses were used to pinpoint more precisely the cause of this volume dilatation process.

SEM examination of fracture surfaces showed that there is extensive cavitation on the fracture surface of BrXP-50 elastomer modified PA-6 (*Figures 7* and *8*). On the fracture surface of a specimen containing 5 wt% BrXP-50 elastomer tested at 25°C, it can be seen that plastic stretching starts from the notch tip and covers the entire fracture surface (*Figure 7a*). At a higher magnification it can be seen that cavitation starts from just ahead of the notch tip (*Figure 7b*), and is associated with an adventitious flaw serving as the nucleation site (*Figure 7c*). However, no cavity was observed near the sides of the same specimen (*Figure 7d*). The underlying importance of cavitation occurring in the middle portion of the specimen but not near the side surfaces is that it indicates that cavitation and subsequent plastic dilatation are a result of the hydrostatic tensile stress, and are not due to plastic shear or tearing. Near the side surfaces of the specimen the plastic shear and tearing are stronger than in the middle portion of the specimen, but no cavitation or dilatation is seen because transverse constraint cannot occur on a free surface. A comparison of the specimen in *Figure 7* with one fractured at a low

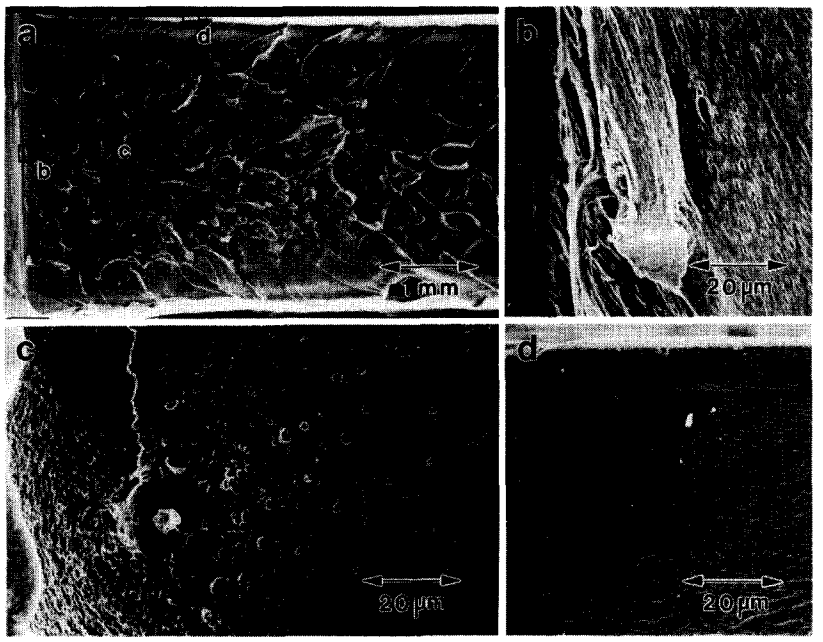

Figure 7 SEM micrographs of the fracture surface of a PA-6/BrXP-50 95/5 blend fractured at 25°C. Note that the positions of micrographs (b), (c) and (d) are marked on micrograph (a)

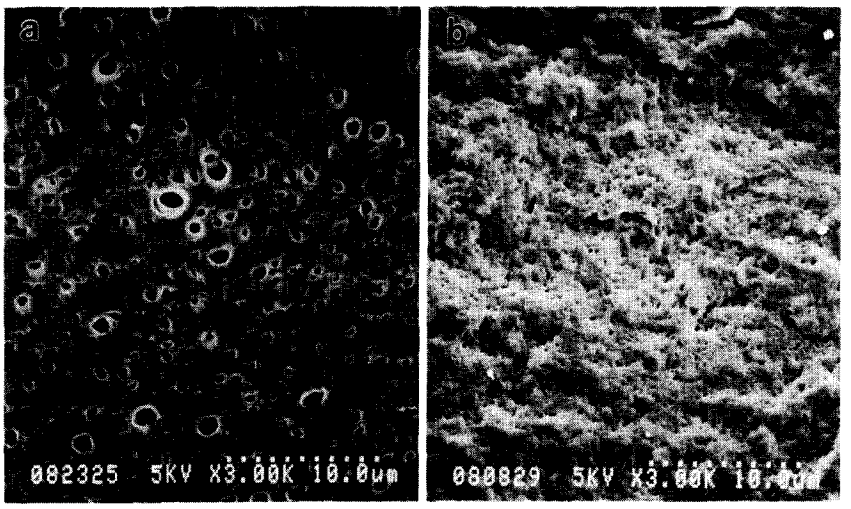

Figure 8 SEM micrographs of the fracture surfaces of PA-6/BrXP-50 95/5 specimens fractured at (a) 25°C and (b) −20°C, with emphasis on BrXP-50 elastomer cavitation

temperature (−20°C) is instructive (*Figure 8*) as it provides a contrast between elastomer particles that have merely cavitated and have little plastic dilatation (−20°C) and those where both processes have occurred (25°C).

To confirm that cavitation and subsequent dilatation is not just a fracture surface phenomenon, we made a TEM examination of microtomed thin sections perpendicular to the fracture surface (*Figure 9*). *Figure 9a* shows that in the undeformed region of a 5 wt% BrXP-50 elastomer modified PA-6 specimen there is no internal cavity in the elastomeric particles. In the whitened region of the same specimen, however, cavitation inside the BrXP-50 elastomer particles is clearly seen (*Figure 9b*). Although the elastomeric particles are not spherical in shape, their internal cavities are spherical or ellipsoidal, reflecting the effects of volume dilatation. No matrix crazing has been found.

In summary, SEM and TEM studies have shown that the volume dilatation process causing the strong light scattering is cavitation introduced by BrXP-50 elastomer modification.

Sequence and importance of events in the damage zone. From the above analyses, it is clear that both matrix shear yielding and cavitation introduced by BrXP-50 elastomer occurred in the impact damage zone. The following is an attempt to deduce the sequence of deformation events and their relative contributions.

Thin sections of the pressurized half of the specimen and its unpressurized counterpart (see *Figure 6*) were made following the same petrographic polishing procedure, and the thin sections thus obtained were viewed using the optical microscope with or without crossed polarizers. The micrographs from these observations are shown in *Figure 10*. Without crossed polarizers, the damage zone of the unpressurized half shows very strong light scattering (*Figure 10a*), while the pressurized half of the specimen has a very similar

appearance to the undeformed region – there is no strong light scattering at all (*Figure 10c*). With crossed polarizers, only a thin layer of birefringence can be seen at the surface of the unpressurized half (*Figure 10b*), similar to that observed in 5 wt% BrXP-50 elastomer modified PA-6 (*Figure 5d*), while a distinctive birefringent zone appears in the pressurized half of the specimen (*Figure 10d*). This zone is elongated, and is much wider than the thin layer of birefringence in the unpressurized half (*Figure 10b*). However, it is much narrower than the light-scattering zone in the unpressurized sample. Furthermore, a comparison of the sizes of the light-scattering and birefringent zones reveals that the birefringent zone is always confined within the light-scattering zone (*Figures 5* and *10*). Since the birefringent zone is near the fracture surface where the stress is the highest, the volume dilatation process must occur at a lower stress, before the occurrence of the plastic shearing process. The volume dilatation cannot be the result of shear plasticity as is sometimes observed in ductile metallic alloys containing hard particles.

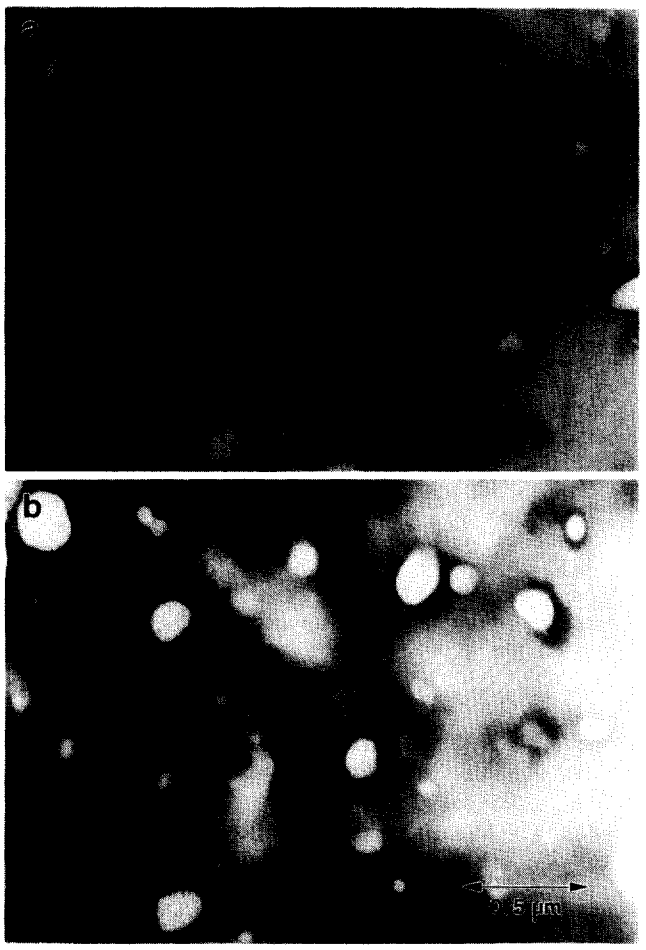

Figure 9 TEM micrographs showing BrXP-50 elastomer cavitation in a PA-6/BrXP-50 90/10 blend

The optical microscopy analyses of both pressurized and unpressurized specimens and the SEM and TEM microscopy analyses lead to the conclusions that: (i) the damage zone of the BrXP-50 elastomer modified PA-6 consists of plastic shearing and elastomer particle cavitation zones; (ii) the plastic shear zone is shorter and narrower than the cavitation zone, indicating that the volume dilatation process occurs first; and (iii) the dilatational energy may be a substantial contribution to the total energy absorption, judging from the size of the cavitation zone. We should further note the critical role played by the notch tip hydrostatic stress which promotes the cavitation. With thinner specimens, or if the specimen does not contain a notch and it is deformed in simple tension, the hydrostatic component would be much lower and cavitation might not occur.

Fracture and toughening mechanisms of pure and BrXP-50 elastomer modified PA-6

Impact fracture mechanism of pure PA-6. In discussing the toughening mechanism of BrXP-50 elastomer modified PA-6, it is useful to understand the fracture mechanism of unmodified PA-6 first. As indicated by the impact strength results in *Figure 1*, unmodified PA-6 is very brittle in standard notched Izod impact tests. The morphology of the impact fracture surface of unmodified PA-6 is shown in *Figure 11*. It is generally flat (*Figure 11a*), with a fracture nucleation site located inside the material (*Figure 11c*), although this is very close to the

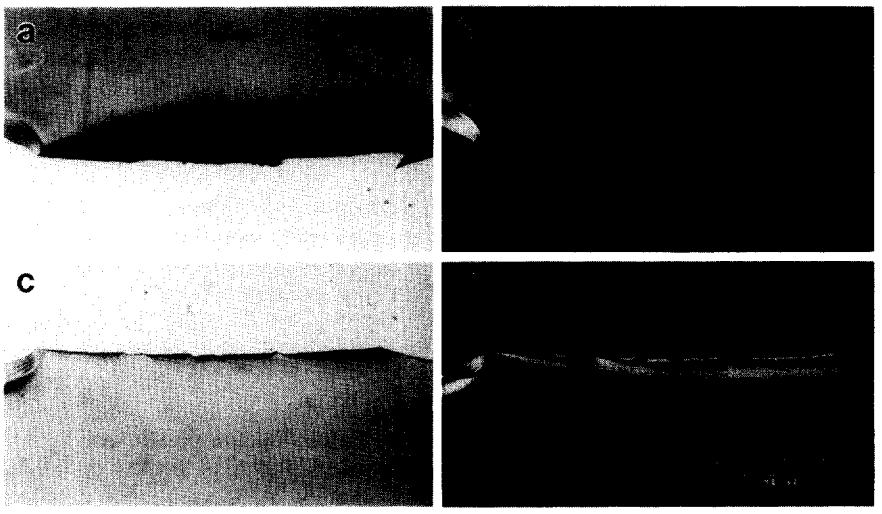

Figure 10 Optical micrographs of thin sections of a PA-6/BrXP-50 70/30 specimen before (a, b) and after (c, d) pressurizing: (a, c) without crossed polarizers; (b, d) with crossed polarizers; specimen fractured at 25°C

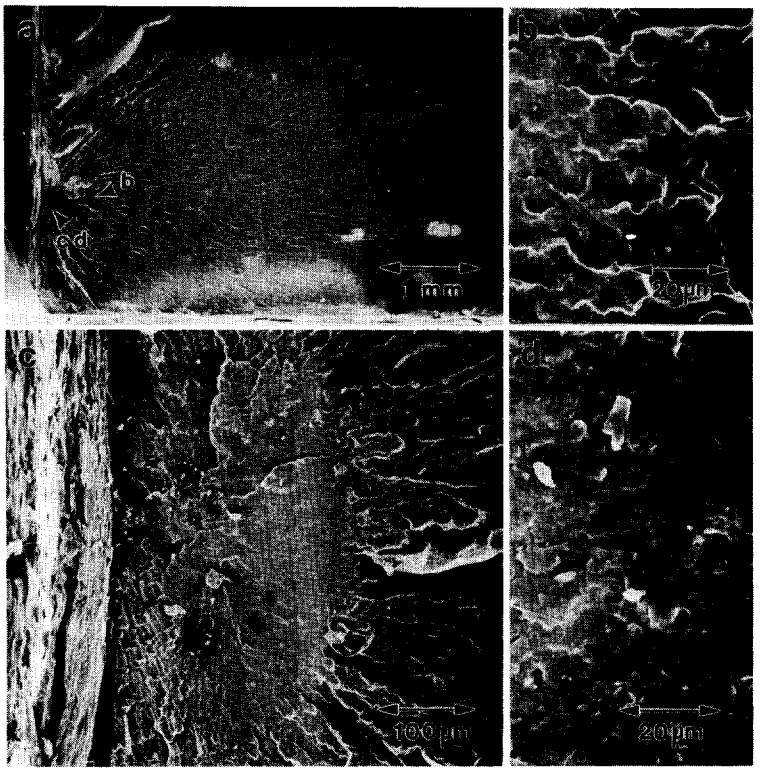

Figure 11 SEM micrographs of the fracture surface of an unmodified PA-6 specimen. Note that the positions of micrographs (b), (c) and (d) are marked on micrograph (a)

notch tip. The crack nucleus is relatively smooth (*Figure 11d*). It is surrounded by a rougher region (*Figure 11b*) where the fracture pattern radiates away from the nucleus. At a distance of a few millimetres from the notch tip the fracture surface becomes smooth once again.

This type of fracture feature is very similar to that reported by Narisawa and Ishikawa[6]. They found that in a plane strain bending test (at low speed) of notched specimens, semicrystalline polymers generally fail in the following sequence of processes: (i) craze nucleation under the constraint, especially the 'plastic constraint' in front of the notch; (ii) craze growth along a plane normal to the major principal stress; and (iii) crack initiation inside the most developed craze that grows along the midplane ahead of the notch and leads to final fracture.

It is now generally recognized that crazes advance by the so-called Taylor meniscus instability[19] and thickening occurs by surface drawing of new materials into the craze fibrils[19–21]. Like the cold drawing of macroscopic polymer fibres, craze fibrils are stabilized at a 'natural' draw ratio, then increase their lengths by continued drawing of new polymer into the neck at the 'shoulders' that separate it from the undrawn polymer outside. In an impact test, it may be impossible for the craze fibrils to grow to the natural draw ratio and keep on drawing new material into the craze. Rather, the fibrils probably break down, and change the craze into a crack.

A critical dilatational stress is proposed by Narisawa and Ishikawa[6] as the criterion for craze nucleation. Furthermore, they found that this critical stress for crack nucleation is nearly constant below the glass transition temperature (T_g). The dilatational stress in front of the notch can be estimated by the slip line field theory[22]. In this theory, the mean stress σ_m, which is the dilatative stress, depends on the material yield stress and the specimen geometry in the following way (for a notch with parallel faces)

$$\sigma_m = \tau_0[1 + 2\ln(1 + x/R)] \quad (1)$$

where τ_0 is the octahedral critical shear stress for yielding, R is the root radius of the notch and x is the distance from the root (see *Figure 12*).

Narisawa and Ishikawa[6] found that the fracture process in PA-6, a semicrystalline polymer with T_g higher than room temperature, also follows the above description in a general manner but there are many fewer crazes. Once formed, the individual crazes grow significantly into the interior of the material and only a few new crazes are formed with increasing load. Although they did not investigate the effect of increasing strain rate, they did investigate the temperature effect on the deformation and fracture of PA-6, and found that as the temperature decreases, the fracture becomes more brittle. The number of crazes also decreases with temperature to only a few well-developed crazes. The low temperature crazes propagate perpendicular to the major stress direction, almost ignoring the spherulitic structure. This scenario, if it applies to impact fracture, should result in a relatively smooth fracture surface containing few fracture steps formed by the lateral merging of many growing crazes.

Based on the work by Narisawa and Ishikawa[6], we can describe the fracture mechanisms of notched, unmodified PA-6 in the Izod impact test as follows.

(i) A small localized plastic zone develops in front of the notch. As the plastic zone grows, a dilatative stress concentration also builds up as a result of the 'plastic constraint'. A 3.2 mm thick Izod testing bar can be in a highly constrained condition if the notch tip is sufficiently sharp and the yield stress is sufficiently high, e.g. at low temperatures or high rates.

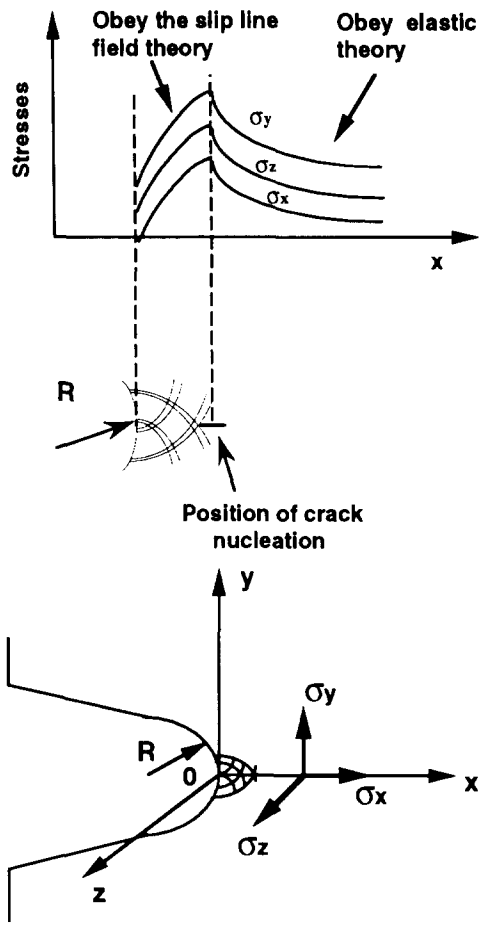

Figure 12 Crazing–cracking mechanism in unmodified PA-6

(ii) When the dilatative stress reaches the critical value, one or more crazes nucleate. Because of the very high local strain rate in the notch tip region (estimated to be several orders of magnitude higher than the conventional tensile test), the yield stress increases; however, according to Narisawa and Ishikawa[6], the critical dilatative stress does not change much. Thus, according to equation (1), a relatively small slip line zone is sufficient to produce a dilatative stress of the critical value. Therefore, the site of craze nucleation is very close to the notch tip. The value of x is estimated to be $0.8R$, based on *Figure 11*, which is substantially smaller than the $x_{max}=2.25R$ allowed by the specimen geometry. Also, the number of crazes is small as a result of the higher strain rate and higher yield stress.

(iii) At such a high strain rate, it is difficult for a craze to maintain stable growth by orientation hardening of interconnecting fibrils and thickening by surface drawing of new materials into the craze fibrils[19–21]. Thus, the craze fibrils soon break down into a crack, which leads to specimen failure.

Toughening mechanism of BrXP-50 elastomer modified PA-6. In explaining the toughening mechanism, it is sometimes stated that the simple reduction of the yield stress of the material will lead to an increase in fracture toughness. The following analysis will show that, while it is true that reducing the yield stress will lead to a slightly larger plastic zone, the increase is not sufficient to explain the experimentally observed substantial increase in the size of the plastic deformation zone and the corresponding impact toughness.

According to the analysis by Narisawa and Ishikawa[6], crazing–cracking will occur when a critical dilatative stress is reached. This critical value does not change with temperature. It is reasonable to assume that it does not change with strain rate, either. Thus, from equation (1), the size of the plastic deformation zone that can be reached before failure is a function of the yield stress of the PA-6 only. If the role of the BrXP-50 elastomer modifier is simply to reduce the yield stress of PA-6, the fracture mechanism of BrXP-50 elastomer modified PA-6 will also be crazing–cracking, and the critical dilatative stress for crazing–cracking will not change. Under these assumptions, the size of the plastic zone of BrXP-50 elastomer modified PA-6 will depend on its yield stress. Since the yield stress of modified PA-6 is lower than that of PA-6, the size of the plastic zone in the modified PA-6 will be larger. At a normal tensile speed (50 mm min^{-1}), the decrease in yield stress due to the addition of 20 wt% BrXP-50 elastomer is 25%. Assuming the same drop in yield stress also occurs at the impact rate, it is estimated by equation (1) that the plastic zone size in 20 wt% elastomer modified PA-6 is about 240 μm. Although this is about twice as large as that in PA-6, it is much smaller than the plastic zone size observed experimentally. At room temperature, plastic deformation covers the entire specimen ligament under the notch in 20 wt% elastomer modified PA-6. Further, the fracture mode is found to be plastic tearing from the notch tip rather than crazing–cracking starting inside the material by the distance estimated above. The above analysis indicates that the role of BrXP-50 elastomer in toughening is not simply to reduce the yield stress of PA-6.

The fracture and toughening mechanism we propose in this paper is a cavitation mechanism. In the impact loading, a plastic constraint will produce a dilatational stress as predicated by the slip line field theory. Under the constraint, the BrXP-50 elastomer particles cavitate before the crazing and fracture of the PA-6 matrix, and lower the dilatational stress by relieving the constraint. As a result of this, the critical dilatational stress required for crazing will not be reached until a later stage of deformation, if at all. We already know that crazing–cracking is the cause of fracture in PA-6; postponing such a process will allow the matrix to undergo more extensive plastic deformation and absorb more energy. This gives rise to a much larger plastic zone and impact strength. If sufficient amounts of BrXP-50 elastomer particles can cavitate and relieve the constraint effectively, then the critical dilatative stress may never be reached and the stress state in front of the notch may reach a plane stress condition. In this stress state, the matrix PA-6 deforms as if it were in uniaxial tension. In this case, maximum plastic energy can be absorbed. Furthermore, instead of a fracture by crazing–cracking controlled by the critical dilatative stress, the fracture mode will be controlled by the ultimate tensile strain of the modified material. Since the local strain is largest at the notch tip, it will reach the ultimate strain of the material first and fail by tearing. This leads to a type of fracture surface morphology wherein plastic tearing covers the entire specimen surface. As the crack propagates, the stress field causes cavitation to occur continuously. This gives rise to a continuous cavitation front as well as a plastic tearing front. *Figure 13* illustrates these processes. Note that four different stages of the crack propagation are shown in the same figure without

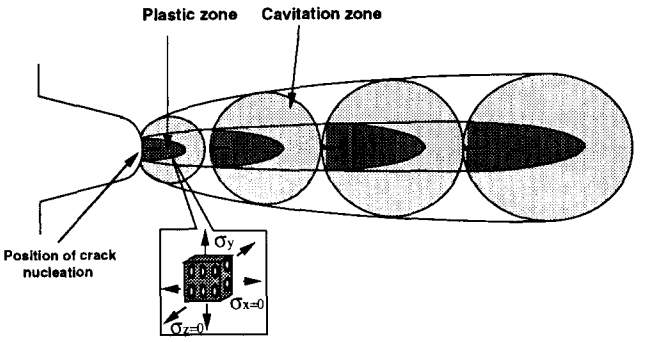

Figure 13 Fracture and toughening mechanisms in BrXP-50 elastomer modified PA-6

the crack-opening and crack-blunting effects. Due to the coexistence and propagation of both zones, the plastic zone is confined within the cavitation zone, as experimentally shown in *Figure 10*.

This cavitation mechanism can also explain the temperature dependence of the impact strength and fracture mechanism. While the critical dilatative stress for crazing is almost constant when the temperature is lower than T_g, the yield stress is very temperature dependent – it increases as the temperature decreases. Based on equation (1), the plastic zone required for creating a critical dilatative stress is reduced, and more effective constraint relief is required to lower the dilatative stress. The same amount of BrXP-50 elastomer effective at causing a change in the fracture mode at room temperature will not be sufficient at a lower temperature, resulting in the return of the crazing fracture mode as the temperature decreases.

CONCLUSIONS

In this paper we have attempted to explain fracture morphology and toughening in terms of the role of the elastomer particles, i.e. cavitation causing relief of plane strain. In two other papers to be published shortly, we will demonstrate how the constraint is affected by the cavitation of elastomeric particles[15], and the inability of elastomeric particles to toughen the polymers if cavitation is suppressed[23]. These papers point out the critical role played by the cavitation of the elastomers.

To summarize this part of our research, we conclude the following.

(i) The fracture mechanism of unmodified PA-6 is crazing–cracking under the dilatational stress created by the plastic constraint.

(ii) The new BrXP-50 elastomer is very effective in toughening PA-6.

(iii) Morphology analysis indicates that cavitation of BrXP-50 elastomer particles occurs in the impact test. The shear deformation of the PA-6 matrix, hence its impact strength, is closely related to the cavitation introduced by BrXP-50 elastomer particles.

(iv) The key function of BrXP-50 elastomer is to cause cavitation in the modified material. A mechanism is proposed wherein cavitation of BrXP-50 elastomer particles is a controlling step in toughening: it relieves the plastic constraint and lowers the mean stress so that the cracking process is postponed and additional plastic deformation can occur, leading to more plastic energy absorption and higher impact toughness.

(v) Plastic dilatation after cavitation may also contribute substantially to the energy absorption.

ACKNOWLEDGEMENTS

The authors gratefully acknowledge the contributions of coworkers at the Exxon Chemical Company, namely C. W. Degener, A. Anastasio, P. J. Chiusano and D. Kauchak in carrying out the compounding works, and K. S. Campo in specimen preparation and preliminary microscopy. D. Li and A. F. Yee also thank the Exxon Chemical Company for an unrestricted grant which made this and other research possible.

REFERENCES

1 Yu, T. C., Wang, H. C., Powers, K. W. and Yee, A. F. *ANTEC Proc. Soc. Plast. Eng.* Detroit, May 1992, p. 2385
2 Wang, H. C. and Powers, K. W. *Rubber Div. Meet. Am. Chem. Soc.* Toronto, May 1991, paper no. 50
3 Yee, A. F. and Pearson, R. A. *J. Mater. Sci.* 1986, **21**, 2462
4 Garg, A. C. and Mai, I.-W. *Composites Sci. Technol.* 1988, **31**, 179
5 Kinloch, A. J. and Young, R. J. 'Fracture Behavior of Polymers', 2nd Edn, Elsevier Applied Science, London, 1985, p. 42/ff
6 Narisawa, I. and Ishikawa, M. *Adv. Polym. Sci.* 1990, **92/93**, 353
7 Wu, S. *J. Polym. Sci., Polym. Chem. Edn* 1983, **21**, 699
8 Ramsteiner, F. and Heckmann, W. *Polym. Commun.* 1985, **26**, 199
9 Hobbs, S. Y., Bopp, R. C. and Watkins, V. H. *Polym. Eng. Sci.* 1983, **23**, 1983
10 Wu, S. *Polymer* 1985, **26**, 1855
11 Oxborough, R. J. and Bowden, P. B. *Philos. Mag.* 1974, **30**, 171
12 Borggreve, R. J. M., Gaymans, R. J. and Schuijer, J. *Polymer* 1989, **30**, 71
13 Oshinski, A. J., Keskkula, H. and Paul, D. R. *Polymer* 1992, **33**, 268
14 Oshinski, A. J., Keskkula, H. and Paul, D. R. *Polymer* 1992, **33**, 284
15 Yee, A. F., Li, D. and Li, X. *J. Mater. Sci.* in press
16 Parker, D. S., Sue, H.-J., Huang, J. and Yee, A. F. *Polymer* 1990, **31**, 2267
17 Ban, L., Doyle, M. J., Disko, M. M. and Smith, G. R. *Polym. Commun.* 1989, **29**, 163
18 Borggreve, R. J. M., Gaymans, R. J. and Eichenwald, H. M. *Polymer* 1989, **30**, 78
19 Kramer, E. J. *Adv. Polym. Sci.* 1983, **52/53**, 1
20 Lauterwasser, B. D. and Kramer, E. J. *Philos. Mag. A* 1979, **39**, 469
21 Donald, A. M., Kramer, E. J. and Bubeck, R. A. *J. Polym. Sci., Polym. Phys. Edn* 1982, **20**, 1129
22 Hill, R. 'The Mathematical Theory of Plasticity', Oxford University Press, London, 1950
23 Li, D., Yee, A. F. and Takahashi, K. *J. Mater. Sci.* in press